lem. Also, cumulative effects of inefficiencies in each of the primer extension reactions may necessitate that the growing result DNA strand be isolated, possibly amplified by PCR, and the reaction continued in a new test tube or tubes containing components required for the remaining steps in the algorithm.

The first generation addition algorithm described here has an obvious limitation. Because the output is encoded in a different form than the input, it is not presently possible to perform either iterative or parallel addition. The development of a more mature DNA-based addition algorithm will require modification of the present procedure to take full advantage of the enormous potential of DNA to engage in massively parallel reactions.

Other aspects of the present algorithm deserve comment: (i) The operator corresponding to the second digit at the 2^0 position plays a special role, because no primer extension reaction would occur without this DNA strand. This operator thus initiates a horizontal chain reaction, involving multiple sequential reactions that ultimately yield the final result strand (*7*). (ii) The amount of DNA required to perform this algorithm does not rise exponentially with the number of digits *n* in each of the two numbers to be added, but is only a linear function of *n*. For large *n*, where end effects of the 2^0 position and the placeholder strand can be ignored, representation of each of the two numbers to be added requires 2.5*n* DNA strands. (iii) The algorithm described here is not technically demanding, because the simple biochemical procedures involved require approximately 1 or 2 days of laboratory work.

Finally, a distinctive aspect of this algorithm is the production in each reaction of a successively elongated result DNA strand that serves a dual function in the addition operation. One role of the result strand is to record, in the proper order, the result of each reaction in the operation. In this sense, the growing result strand is analogous to a passive tape on which the outcome of successive operations is written, yielding finally an output tape that encodes the result of the addition operation. However, the growing result strand is also an active participant in the addition algorithm because the output result strand for each operation (reaction) serves as the operator (primer) for the succeeding operation. Thus, the result DNA strand serves both as an operator that transfers information during the addition algorithm and as a tape that records the outcome of this algorithm.

REFERENCES AND NOTES

1. L. M. Adleman, *Science* **266**, 1021 (1994).
2. R. J. Lipton, *ibid.* **268**, 542 (1995).
3. J. H. Reif, in *Seventh Annual ACM Symposium on Parallel Algorithms and Architectures (SPAA95)*, Santa Barbara, CA, June 1995, pp. 213–223.
4. F. M. Ausubel *et al.*, Eds., *Short Protocols in Molecular Biology* (Wiley, New York, ed. 3, 1995).
5. F. Guarnieri and C. Bancroft, in *Proceedings of the Second Annual Meeting on DNA Based Computers*, Princeton, NJ, 10 to 12 June 1996 (American Mathematical Society, Providence, RI, in press).
6. The elements illustrated in Fig. 3 were represented by the following sequences (all listed 5′ to 3′) or the appropriate complementary sequence (or both): $\overline{0}$, CCTTACCCCTTTCTACCTCT; DEF, TCGTCTCAGGGGGGGTGCTT; $\overline{1}$, CACGAAACGAGCGAAAGCACCCACAACAAGAACCACACAGCACAACCAGA; OPP, GACCAAATACAGGCTAACAT; $\overline{PP}$, CATTCCCCTTCCTCTCCTCC; and J, TCTCC. Each primer extension reaction indicated in Fig. 3A was performed by first combining the following reagents in a final volume of 30 μl: supplemented extension buffer [AmpliTaq buffer (Perkin-Elmer), supplemented with 2.5 U AmpliTaq enzyme, 2.5 mM $MgCl_2$, deoxyadenosine triphosphate (dATP) and deoxythymidine triphosphate (dTTP) (each 0.2 mM)], [^{32}P]deoxycytidine triphosphate (dCTP) and [^{32}P]deoxyguanosine triphosphate (dGTP) (each 3000 Ci/mmol), and two DNA strands representing the first number (50 ng each) plus 5 μg of the second number strand. Then for primer extension, reactions were processed for 15 cycles each at 95°C for 1 min, 58°C for 1 min (except for 0 + 1, at 66°C for 1 min), and 72°C for 20 s. Except for 1 + 1, the primer extension reactions indicated in Fig. 3B were the same, except that the [^{32}P]dCTP plus the other three unlabeled deoxynucleotide triphosphates were present. The first 1 + 1 reaction (indicated in Fig. 3A) was also done as described above, except that only dATP, dTTP, and dGTP were present (note that the extended sequence should contain no Cs). After this reaction, 3 μl of the reaction were combined with 5 μg of the 5′ 1/PP/J 3′ DNA strand (Fig. 3B) [brought to a total volume of 30 μl with supplemented extension buffer as described above (but also containing dGTP)] and [^{32}P]dCTP and subjected to primer extension as above. For all reactions indicated in Fig. 3, samples were then denatured and analyzed by standard denaturing gel electrophoresis [J. Sambrook, E. F. Fritsch, T. Maniatis, *Molecular Cloning* (Cold Spring Harbor Laboratory, Cold Spring Harbor, NY, ed. 2, 1989), p. 13.45)], except that the sample buffer contained in addition 10 mM NaOH. For the analysis shown in Fig. 4, the following denatured (and therefore single-stranded) ^{32}P-labeled molecular size markers were used: (A) Msp I–digested plasmid pBR322; (B) strands $\overline{PP}/\overline{0}/\overline{OPP}$ and $\overline{1}/\overline{DEF}$ (60 and 70 bases, respectively) plus oligomers of the 41 base–long 1P element [G.-Z. Yan, W. T. Pan, C. Bancroft, *Mol. Endocrinol.* **5**, 535 (1991)]. Differences in the efficiencies of individual primer extension reactions were corrected for by applying approximately equal amounts of product. After electrophoresis, the gel was fixed, dried, and imaged by autoradiography and scanning.
7. The horizontal chain reaction described here may find application in a number of areas of computation; for example, in the development of a one-dimensional DNA cellular automaton. We are currently investigating how the horizontal chain reaction concept may be used to develop a DNA-based simulation of a Turing machine.
8. Supported by funds provided by The Mount Sinai School of Medicine. We thank an anonymous reviewer for helpful comments on the manuscript.

26 March 1996; accepted 3 May 1996

Maya Blue Paint: An Ancient Nanostructured Material

M. José-Yacamán,* Luis Rendón, J. Arenas,
Mari Carmen Serra Puche

Maya blue paint was often used in Mesoamerica. The origin of its color and its resistance to acids and biocorrosion have not been fully understood. High-resolution transmission electron microscopy, electron energy loss spectroscopy, and x-ray microanalysis studies of authentic samples show that palygorskite crystals in the paint form a superlattice that probably occurs as a result of mixing with indigo molecules. An amorphous silicate substrate contains inclusions of metal nanoparticles encapsulated in the substrate and oxide nanoparticles on the surface. The beautiful tone of the color is obtained only when both the particles and the superlattice are present.

When studying Mayan archeological sites, researchers are always stunned by the blue color often used in pottery, murals, and ceremonial artifacts. The color first described in the Chichén Itza ruins by Merwin (*1*) was named Maya blue by Gettens (*2*). This color differs from any blue ever identified on ancient or medieval paintings from Europe or Asia. It is not based on copper or on ground lapis lazuli or lazurite, which are common in European and Asian paintings (*3*). Maya blue was used in Mesoamerica and colonial Mexico probably as late as the 20th century (Fig. 1). In addition to its beautiful look, Maya blue is resistant to diluted mineral acids, alkalis, solvents, oxidants, reducing agents, moderate heat, and even biocorrosion. Paintings in the Bonampak archeological site have retained their blue color after centuries in the extreme conditions of the rain forest.

The structure of the material and the origin of the Maya blue color have been debated extensively. Maya blue contains clays (mainly palygorskite mixed with

---

M. José-Yacamán and L. Rendón, Instituto de Física, Universidad Nacional Autónoma de México, Apdo. Postal 20-364, Delegación Alvaro Obregón, 01000 México, D.F., México.

J. Arenas, Instituto Nacional de Investigaciones Nucleares, Carr. México-Toluca Km. 36.5, 52045 Salazar Edo. de México.

M. C. Serra Puche, Museo Nacional de Antropología, Instituto Nacional de Antropología e Historia, Paseo de la Reforma y Gandhi s/n, Polanco, 11560 México, D.F., México.

*To whom correspondence should be addressed. E-mail: yacaman@sysul1.ifisicacu.unam.mx

smaller amounts of sepiolite and montmorillonite), but these clays are white powders. Van Olphen (4) described a procedure to produce a pigment with properties similar to those of Maya blue. Palygorskite is dyed with synthetic indigo ($C_{16}H_{10}N_2O_2$) and heated at ~150°C for 20 hours. Indigo existed in pre-Columbian America and has been identified in pre-Columbian textiles (5). According to Torres (3), a dye called añil was obtained from the sprigs of a plant called xiuquilit (indigophera sp.); in the 17th century, the production of indigo in New Spain was very important. Indigo dissolves in nonpolar solvents and dyes but is not resistant to either acids or biocorrosion; therefore, the question remains as to why mixing the clay and the organic compound produces an acid-resistant blue coloration.

We studied Maya blue paint with high-resolution electron microscopy, scanning electron microscopy (SEM) coupled with x-ray microanalysis, electron energy loss spectroscopy (EELS), and electron diffraction (6). Samples were ground and cleaned with an organic solvent in an ultrasound bath. Transmission electron microscopy (TEM) was performed on uncoated samples with a JEOL 4000-EX microscope with a point resolution of ~0.17 nm, as was the SEM. Some of the images were computer processed to increase the signal-to-noise ratio. A Fourier transform from the digital image was obtained, and a mask was applied to some areas. A second Fourier transform recovered the original image in which noise had been reduced.

Six samples from Jaina Island (7) and two samples from Palenque were examined; all eight corresponded to the late classical period. A few milligrams of different samples were obtained from the collection at the National Anthropology Museum of Mexico and directly from the Palenque archeological site.

The x-ray analysis, with a spot size of several micrometers, revealed the elements expected for palygorskite—magnesium, silicon, aluminum, and oxygen—but in addition, a prominent peak of iron was seen. Examination of the sample with TEM showed that at the microscopic level, the samples consisted of a mix of two regions (Fig. 2). The first region contained crystals with a well-defined form, usually plate- or needle-shaped (marked A in Fig. 2); the second region was composed of an amorphous solid that contained small particles with nanometer dimensions (marked B in Fig. 2).

The needle-shaped crystallites were identified by electron diffraction and x-ray microanalysis as palygorskite. The chemical composition of the sample was close to $Mg_5(Si,Al)_8O_{20}(OH)_2{\cdot}8H_2O$. Atomic-resolution images (Fig. 3) show a periodic feature larger than the expected lattice distance on the crystallites: The larger period corresponds to ~14 Å, about three times the lattice spacing in the ⟨400⟩ direction (d_{400}), and therefore indicates a superlattice. Almost 90% of the needles show the superlattice structure. This kind of superlattice was not observed in control samples of palygorskite that were not mixed with indigo, which suggests that impurities are stacked inside the pillared palygorskite structure. Intercalation of indigo molecules might explain the corrosion resistance.

Fig. 1. Maya blue was used in this mural representing a quetzal obtained from the Cacaxtla (Mexico) archeological site.

However, the material is more complex: An irregularly shaped substrate that contained metal particles on the surface was buried in the bulk of the clay (marked B in Fig. 2). The nanometer-sized particles had a well-defined shape and crystalline structure (Fig. 4). The substrate was basically amorphous SiO_2. Important differences in the nanoparticle structure among samples from different archeological sites were observed. Particles in samples from Jaina Island are uniform in shape and approximately spherical (Fig. 4A). The EELS spectra from these particles indicate that they are composed of Fe, Cr, Mn, Ti, and V; most of the particles are Fe and Cr. We made a detailed analysis of the structure of the particles using image processing (Fig. 4B). Particles show twin boundaries and other planar defects (Fig. 4C). Electron microdiffraction measurements from individual particles indicate that some particles were in a metallic state, whereas others correspond to oxides: for example, Fe_2O_3 was often found. The particles in a metallic state were encapsulated inside the substrate, but the oxidized particles were on the surface. Some of the particles were coated with an oxide film on the surface, whereas others were fully oxidized. The size distribution of oxide nanoparticles was very narrow (a mean value of 4.0 nm and a standard deviation of 0.6 nm).

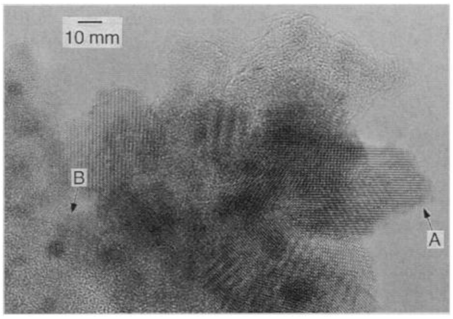

Fig. 2. General image of a sample of Maya blue from Jaina Island. Several regions can be identified: (A) clay and (B) silicate with metal particles.

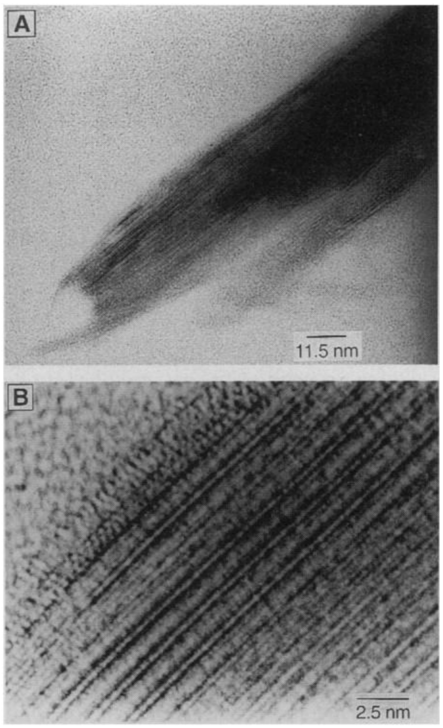

Fig. 3. Palygorskite crystals. (**A**) Needle shape of the crystals. (**B**) High-magnification image of a crystal showing a superlattice period of about 1.4 nm.

Samples from Palenque are similar to the ones from Jaina and also show needles of palygorskite and nanoparticles supported in an amorphous SiO_2 substrate. However, the particles have a broader size distribution and in many cases contain well-defined facets. The majority of the nanoparticles are once again Fe, with a minor proportion being Cr, Ti, and Mn. The SiO_2 substrate contains Na and Mg impurities. Electron diffraction patterns indicate that there are several preferential orientations of the nanoparticles with respect to the substrate,

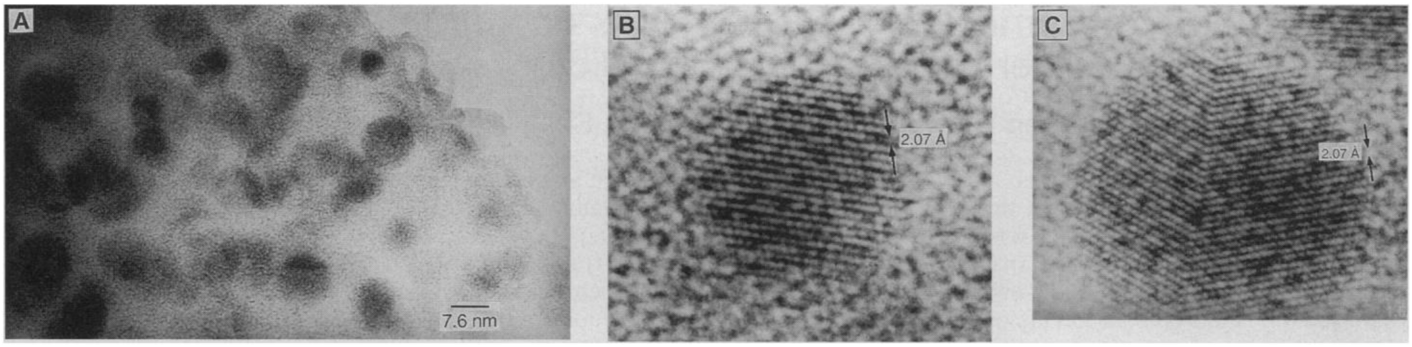

Fig. 4. (**A**) Small metallic and oxide particles on an amorphous SiO_2 support. (**B**) Atomic-resolution image of a particle showing its cubo-octahedral shape. (**C**) High-resolution image of a metallic particle showing a twin boundary along the (100) planes.

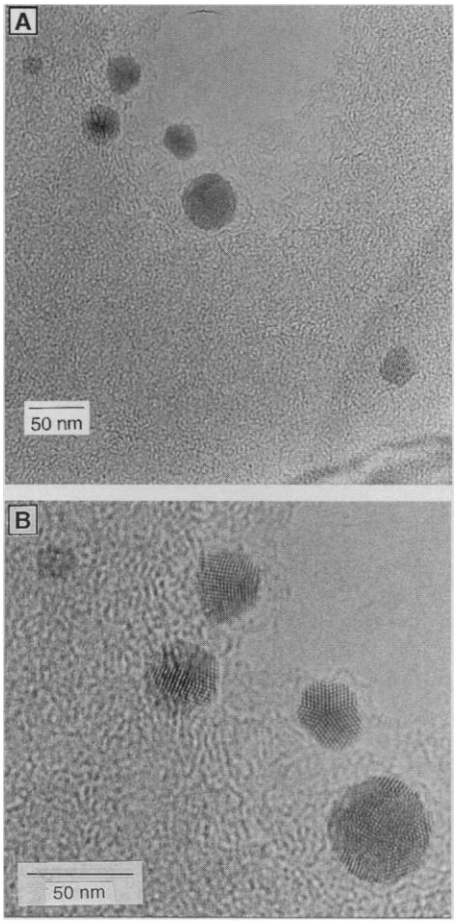

Fig. 5. (**A**) High-resolution image of synthetic Maya blue produced by heating añil (indigo containing impurities) and Sacalum clay. Several metal particles can be observed on the clay support. (**B**) Magnification of upper right portion of (A).

which indicates a strong interaction between the nanoparticles and the substrate.

In early reports of Maya blue, Gettens (*2*) found 0.5 to 1.0% impurities of Fe and 0.005 to 0.01% of Mn and Cr. These impurities were disregarded because of their low concentration. However, metallic and oxide particles of nanometer dimensions can strongly influence the optical properties of a material, and small impurity concentrations are sufficient to produce particles. Nanoparticles can have both linear and nonlinear optical properties (*7*). Linear absorbance of small particles can create a resonance feature related to surface-plasmon excitation. In many cases, classical Mie theory adequately describes the optical properties (*8*). The main effect of the particles is classical in nature, although quantum effects are not excluded. Particles much smaller than the wavelength of the visible light (as is the case for Maya blue) have an extinction spectra dominated by the imaginary part of the refractive index. The blue color comes from an absorption curve peaked in the visible part of the spectrum. The oxide metals can account at least in part for the color. In addition, many of the particles are nonspherical, and planar defects may play an important role in the optical properties. The color of Maya blue could be at least partially associated with the presence of nanoparticles. Littmann (*9*) showed that the color of the crystallites in the paint samples changed from blue to yellow-green upon dispersion of the powder. A classical example of this effect are the gold colloids for which the color changes from blue to yellow-green with changing particle size, an effect originally described by Faraday (*10*).

This discussion still does not tell us the source of the metal. There is an ancient mine in the Mayan region in a city called Sacalum, near Mérida (*11*); this mine may have provided the clay material for the Maya blue paint. We obtained a sample of Sacalum clay from the ancient mine. Our x-ray microanalysis and x-ray and electron diffraction showed that the mineral contained palygorskite combined with Ca and Mg oxides and carbonates and impurities of Fe, Ti, and Mn. We heated a sample to 100°C for 12 hours, and the color changed from white to light red. This change probably resulted from the precipitation of impurities to the surface (*12*). However, this procedure alone does not reproduce Maya blue. We then heated the Sacalum clay in añil at 100°C according to pre-Hispanic methods (*13*). This procedure fully reproduced the Maya blue microstructure (Fig. 5); x-ray microanalysis of the añil sample indicated that it contained impurities mainly of Fe. It is likely that impurities were added to the indigo during the preparation of the añil; therefore, the main source of the metallic particles was probably añil. Maya blue may be similar to colorants used around the same time in Europe. Oxidization or encapsulation of particles in the substrate explains the acid-resistant character of the paint. The indigo molecules encapsulated in the palygorskite pores probably also contribute to the final color. The combination of an intercalated clay forming a superlattice and the metallic and oxide nanoparticles supported on an amorphous substrate makes the ancient Maya blue look like modern nanostructured materials.

REFERENCES

1. H. W. Merwin, in *The Temple of the Warriors*, E. H. Morris, J. Charlot, A. A. Morris, Eds. (Publication 606, Carnegie Institution of Washington, Washington, DC, 1931), contribution 60.
2. P. Gettens, *Am. Antiq.* **27**, 557 (1962).
3. L. Torres, in *Materials Issues in Art and Archeology*, E. Sayze, P. Vandiver, J. Druzik, C. Stevenson, Eds. (MRS Symposium Proc. 123, Materials Research Society, Pittsburgh, 1968), pp. 123–128.
4. H. Van Olphen, *Science* **154**, 645 (1966).
5. L. Torres, *An. INAH A* **7**, 260 (1974).
6. B. Repetto, *Bol. INAH* **14**, 51 (1975).
7. J. W. Bloemer, J. Haus, P. R. Ashley, *J. Opt. Soc. Am. B* **7**, 790 (1990).
8. H. C. Van de Hulst, *Light Scattering by Small Particles* (Dover, New York, 1981).
9. E. Littmann, *Am. Antiq.* **47**, 404 (1982).
10. M. Faraday, *Philos. Trans.* **147**, 145 (1857).
11. D. Arnold and B. F. Bohor, *Archaeology* **28**, 23 (1975).
12. M. José-Yacamán and E. Pedrero Nieto, *J. Cryst. Growth* **7**, 3 (1970).
13. C. Reyes Valerio, *The Bonampak al Templo Mayor* (Azul Maya en Mesoamerica Siglo XXI, Mexico City, Mexico, 1993).

13 November 1995; accepted 4 April 1996